Glacier Variations in the Fedchenko Basin, Tajikistan, 1992–2006: Insights from Remote-sensing Images

Authors: Zhang, Qibing, Kang, Shichang, and Chen, Feng

Source: Mountain Research and Development, 34(1) : 56-65

Published By: International Mountain Society

URL: https://doi.org/10.1659/MRD-JOURNAL-D-12-00074.1

Mountain Research and Development (MRD)
An international, peer-reviewed open access journal
published by the International Mountain Society (IMS)
www.mrd-journal.org

MountainResearch
Systems knowledge

Glacier Variations in the Fedchenko Basin, Tajikistan, 1992–2006

Insights from Remote-sensing Images

Qibing Zhang[1,3], Shichang Kang[1,2], and Feng Chen[1]*

** Corresponding author: ahsszqb@itpcas.ac.cn*

[1] Key Laboratory of Tibetan Environment Changes and Land Surface Processes, Institute of Tibetan Plateau Research, Chinese Academy of Sciences, Lin Chui Road, Beijing 100101, China

[2] State Key Laboratory of Cryospheric Sciences, Cold and Arid Regions Environmental and Engineering Research Institute, Chinese Academy of Sciences, 320 Donggang West Road, Lanzhou 730000, China

[3] University of Chinese Academy of Sciences, Beijing 100049, China

The Fedchenko glacier system harbors the longest glacier (77 km) outside of the polar areas. It has a great influence on the local economy and ecology as a water resource. The glacier area in the Fedchenko basin was investigated using Landsat TM images in 1992, Landsat ETM+ images in 2000, and ALOS/AVNIR2 images in 2006. The total area was 835.9 km^2 in 1992, 830.0 km^2 in 2000, and 864.8 km^2 in 2006, increasing by 3.46% from 1992 to 2006 (an average rate of 0.25% per year). The Fedchenko glacier system is relatively stable when considering glacier surging and data errors. Reanalysis data (eg for temperature and precipitation) from the US National Centers for Environmental Prediction and National Center for Atmospheric Research suggest that increasing precipitation since 1990 probably caused the slight change in glacier area.

Keywords: *Fedchenko glacier system; remote sensing; glacier area; climate change.*

Peer-reviewed: *September 2013* ***Accepted:*** *October 2013*

Introduction

Glaciers are sensitive indicators of climate change (Oerlemans 1994, 2001; Haeberli 1995; Kang et al 2010). Variations in glacier area, length, thickness, equilibrium line altitude (ELA), flow velocity, and surface albedo are mainly caused by climate change (Haeberli 1995; Oerlemans 2001; Cuffey and Paterson 2010). Remote-sensing images can be used to detect changes in glacier area (Paul et al 2007; Andreassen et al 2008; Bolch, Menounos, et al 2010), length or terminus position (Haritashya et al 2009; Lopez et al 2010), and thickness (Kääb 2008; Willis et al 2012). The driving factor of geometric change is glacier mass balance, which is correlated to ELA or accumulation area ratio (Braithwaite 1984; Kulkarni 1992; Racoviteanu, Williams, et al 2008; Braithwaite and Raper 2009).

Most glaciers (surging and nonsurging) on the Karakoram Mountains are advancing or stable, which is consistent with the gain of mass during 2000 to 2008 (Gardelle et al 2012). An increase in winter precipitation since 1961 is a potential source of greater accumulation in the upper parts of glaciers (Gardelle et al 2012). The eastern Pamir also show positive mass balance, which has been attributed to increasing precipitation since 1979, due to strengthened westerlies (Yao et al 2012). Glacier investigations in the Pamir Plateau are still scarce, especially for the Fedchenko glacier system (Kutuzov and Shahgedanova 2009).

Generally, the foothills receive less precipitation, while mountains with high elevation can intercept water vapor carried by westerlies, store it in the form of glaciation, and release water by glacier melting. Water from glaciers irrigates farmland and supplies other anthropogenic activities in the arid area of the Pamir region (Barnett et al 2005). Thus, there is an urgent need to investigate the variation of glaciers in the region under ongoing climate change and accurately evaluate its effect on local water resources (Kutuzov and Shahgedanova 2009). This article investigates variations in glacier area in the Fedchenko basin from 1992 to 2006 and discusses the relationship between glacier variation and climate change.

Study area

The extent of the Fedchenko glacier system (38°50′N; 72°15′E) (Figure 1A) has been estimated in different ways, including 649 km^2 by Aizen et al (2009) and 992 km^2 by the Japan Aerospace and Exploration Agency (2006). This study defines the Fedchenko glacier system based on a specific pour point (Figure 1B). The system contains

FIGURE 1 The Fedchenko glacier system: (A) location; (B) constitution; and (C) partial map of delineation on an ETM+ image. Threshold for NDSI is 0.5; 1 and 2 refer to the debris-covered glaciers, which were manually delineated; 3 and 4 refer to seasonal snow, which was erased from the image. A false-color composite image (bands 5, 4, and 3) of ETM+ appears in the background.

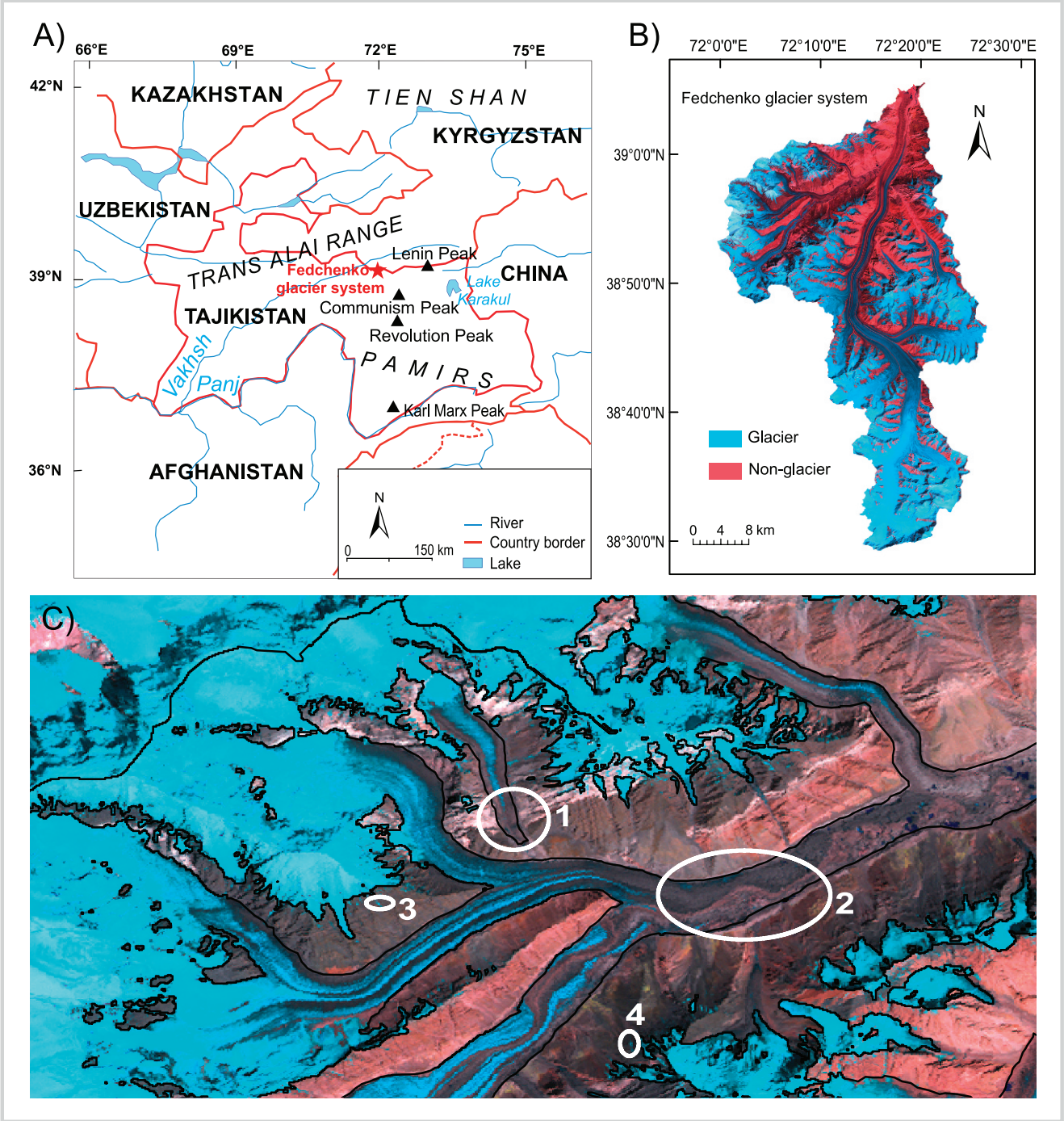

many tributary glaciers, such as the Bivouac and Nalifikin glaciers, as well as many glaciers that have been disconnected since the Little Ice Age. The longest alpine dendrite glacier outside of the polar regions, the Fedchenko glacier system has a length of 77 km, an elevation of 2900–6300 m above sea level (asl) (Aizen et al 2009), and an average ELA of 5000 m asl. In the system, many dark-brown debris-covered glaciers and surging lobes can be found on Landsat Enhanced Thematic Mapper plus (ETM+) remote-sensing images in a composite of bands 5, 4, and 3 (Figure 1C). In winter, moisture comes from the Atlantic Ocean and contributes

http://dx.doi.org/10.1659/MRD-JOURNAL-D-12-00074.1

TABLE 1 Characteristics of the satellites and sensors used.

	Satellite sensor		
	Landsat 5 TM[a)]	Landsat 7 ETM+[a)]	ALOS/AVNIR2[a)]
Spectral band			
Blue	1: 0.452–0.518 μm	1: 0.452–0.514 μm	1: 0.420–0.500 μm
Green	2: 0.528–0.609 μm	2: 0.519–0.601 μm	2: 0.520–0.600 μm
Red	3: 0.626–0.693 μm	3: 0.631–0.692 μm	3: 0.610–0.690 μm
Near infrared	4: 0.776–0.904 μm	4: 0.772–0.898 μm	4: 0.760–0.890 μm
Shortwave infrared	5: 1.567–1.784 μm 6: 10.45–12.42 μm 7: 2.097–2.349 μm	5: 1.547–1.748 μm 6: 10.31–12.36 μm 7: 2.065–2.346 μm PAN: 0.515–0.896 μm	
Spatial resolution	TIR[a)]: 120 m Other: 30 m	TIR[a)]: 60 m PAN[a)]: 15 m Other: 30 m	10 m
Coverage	185 × 185 km	185 × 185 km	70 × 70 km
ID of scene used scene	203–168	038–722	North/south ALAV2A033722810/20
Path/row	151/033	151/033	196/2810 (frame) 196/2820 (frame)
Data acquisition date	27 September 1992	24 August 2000	12 September 2006
Source	GLCF[a)]	GLCF[a)]	RESTEC[a)]

[a)]TM, Thematic mapper; ETM+, Enhanced Thematic Mapper plus; ALOS, Advanced Land Observing Satellite; AVNIR2, Advanced Visible and Near Infrared Radiometer Type 2; PAN, panchromatic sensor; TIR, thermal infrared; GLCF, Global Land Cover Facility; RESTEC, Remote Sensing Technology Center of Japan.

the largest yearly amount of precipitation, while summers are dry (Aizen et al 2009), causing glaciers to accumulate in winter and ablate in summer. The ablation season ends in August and September. The Fedchenko meteorological station (4169 m asl; 38.83°N; 72.22°E) operated from 1933 until it was closed in 1994.

The melt water of glaciers flows through the Muksu, Surkhob, Vakhsh, and Amu Darya Rivers, eventually discharging into the Aral Sea. It feeds densely populated and industrial areas along the rivers. Thus, glacier variations in the Fedchenko basin have a great influence on ecology, agriculture, and economic development in these areas. Sustainable strategies, such as encouraging reasonable water consumption and establishing effective irrigation systems, have been carried out along the Amy Darya River (Micklin 2006).

Data and methodology

Landsat and Advanced Land Observing Satellite (ALOS) images were used in this study (Table 1). Landsat Thematic Mapper (TM) and Enhanced Thematic Mapper plus (ETM+) images were available from the Global Land Cover Facility (2013); these images have already been orthorectified to Level 1G products (UTM projection Zone 43N, WGS 1984 datum). The ALOS images with rational polynomial coefficients (RPC) files were bought from the Remote Sensing Technology Center of Japan; they were L01B products and coarsely geometry-corrected. Cloud cover obscured less than 1% of the total image areas; the acquisition time was at the end of the ablation season, and seasonal snow covered the lowest yearly area. Thus, snow and clouds did not greatly affect our ability to extract glacier outlines.

The Shuttle Radar Topography Mission (SRTM) C-band digital elevation model (DEM) with resolutions of 90 m, downloaded from the Consultative Group for International Agriculture Research's Consortium for Spatial Information (2013), was used. SRTM DEM voids were filled and updated to version 4, and the problems of radar shadow, layover, and foreshortening from synthetic aperture radar (SAR) were resolved (Le Bris et al 2011). The Fedchenko basin was defined using SRTM DEM by the hydrology tools in ArcGIS 9.3 software, and then it was used to clip the glacier polygons.

Glaciers react to climate by changing in area; glacier area is easily detectable on remote-sensing images (Paul 2002; Paul et al 2002). Exposed glaciers and snow have high reflectance in the visible and near-infrared (VNIR) band and strong absorption in the shortwave infrared

http://dx.doi.org/10.1659/MRD-JOURNAL-D-12-00074.1

FIGURE 2 Processing method used in this study.

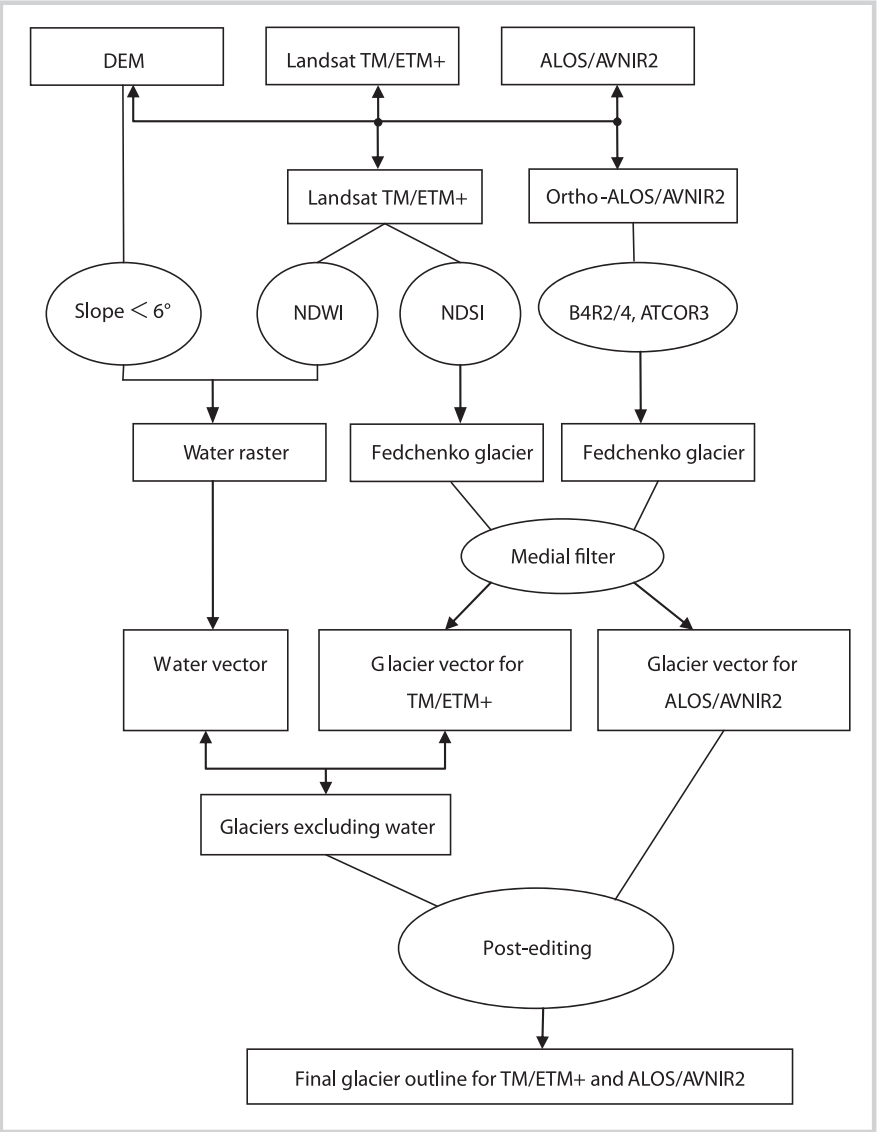

band (SWIR) (Warren 1982; Dozier 1989; Hall et al 1995); therefore, these two bands can be used to extract glacier outlines. TM3/TM5 or TM4/TM5 plus an additional green or blue band and the normalized difference snow index (NDSI) are widely used; this ratio algorithm is a robust method for delineating glaciers in shadow areas and removing cloud covers (Winther 1992; Paul 2002; Paul et al 2002; Racoviteanu, Arnaud, et al 2008). However, water bodies are bracketed, and postediting is necessary (Paul et al 2007; Andreassen et al 2008; Racoviteanu, Williams, et al 2008; Svoboda and Paul 2009). The threshold value for the band ratio can be obtained using a histogram map (Gupta et al 2005; Silverio and Jaquet 2005). The band value can be a raw digital number value (Bayr et al 1994) or reflectance at the top of the atmosphere (Jacobs et al 1997); this digital number value is easier to use and leads to more accurate results (Paul 2000). Small seasonal snow patches and gaps due to debris cover can be reduced using a median filter (Andreassen et al 2008; Racoviteanu, Arnaud, et al 2008). Moraine- and debris-covered glaciers cannot be extracted by the band ratio method (Paul et al 2004); the best way is to manually delineate them with the help of DEM and band composite (Bolch, Menounos, and Wheate 2010).

Methods used in this paper are shown in Figure 2. For Landsat TM/ETM+, strong shadows occurred on the images because of complicated relief, and mapping of the glacier boundaries had to be improved using NDSI = (band 2 − band 5)/(band 2 + band 5). NDSI is robust enough to diminish the topographic effect (Racoviteanu,

http://dx.doi.org/10.1659/MRD-JOURNAL-D-12-00074.1

TABLE 2 Thresholds used for glacier mapping for all sensors.

Sensor	Snow and ice	Snow and ice in shadow
TM/ETM+	NDSI[a] $\geq$ 0.50	Delineate automatically
AVNIR2	10 $\times$ (band 2/band 4) $\geq$ 16.6 and band 4 $\geq$ 58 10 $\times$ (band 2/band 4) $<$ 16.6 and band 4 $\geq$ 121.5	Delineate manually

[a]NDSI, normalized difference snow index.

Arnaud, et al 2008). A threshold value of 0.5 was chosen based on the histogram map (Table 2); the resulting glacier margins match well with those on the false-color-composite images (Figure 1C). Water bodies were identified using the normalized difference water index (NDWI), but turbid lakes and shadowy areas have the same spectral property, and so a logical algorithm of NDWI $\geq$ 0.34 and slope angle $<$ 6° was used to extract water pixels on the image, and then the total area of water body inclusions within the glacier features was subtracted. ETM+ images have a panchromatic band with 15 m resolution; this band can be fused with VNIR of 30 m resolution to get 15-m-resolution images, which can improve the accuracy of delineating debris-covered glaciers.

For the ALOS image, ground-control points for orthorectification were selected directly from the ETM+ image. In total, 14 control points were selected. The ALOS/AVNIR2 image was orthorectified with RPC in ENVI 4.7; the root-mean-square error (RMSE) was 3.6 m within 1 pixel error. NDSI is not applicable to the ALOS/AVNIR2 image because it has no SWIR band, so the B4R2/4 was used from reference to B3R1/3 (threshold for band 3 and the ratio of band 1 to band 3) for Advanced Spaceborne Thermal Emission and Reflection Radiometer (ASTER) images (Kargel et al 2005), because the spectral ranges of band 2 and band 4 of ALOS/AVNIR2 were in agreement with band 1 and band 3 of ASTER, respectively. This algorithm can isolate water bodies and overcome satellite sensor saturation over snow (Raup et al 2007). A two-dimensional scatter plot was drawn using 10 $\times$ (band 2/band 4) and band 4, and glacier threshold values were visually inspected on the two-dimensional scatter plot that was linked to the false-color image of ALOS/AVNIR bands 4, 3, and 2. The constraints for dirty ice were 10R2/4 $\geq$ 16.6 and band 4 $\geq$ 58, whereas for illuminated snow and clean ice, they were 10R2/4 $<$ 16.6 and B4 $\geq$ 121.5 (Table 2).

The glaciers in shadow areas could not be discriminated automatically by logistic algorithm; therefore, the ALOS/AVNIR2 image was topographically corrected with the Sandmeier model (Sandmeier and Itten 1997), which was run in ATCOR3 for ERDAS IMAGINE 2011 software. The key input parameters for the model are scene visibility (km) and water content. Water content was substituted by middle-latitude summer rural provided by the ATCOR3 software, and scene visibility was calculated with aerosol optical depth (τ) obtained by Song's algorithm (Song et al 2001). The path radiance in Song's algorithm was determined by the method described by Chavez (1988). A τ of 0.078122 and scene visibility of 82 km were obtained when the satellite overpassed. Finally, glaciers in shadow were delineated manually on the corrected map.

Postediting was necessary for both images. Small snow patches and gaps were removed using a 5 $\times$ 5 median filter. Glaciers with area smaller than 0.01 km^2, large seasonal snow patches, and remnant water bodies were eliminated. Debris-covered glaciers, missed glaciers in shadow or under cloud, and supraglacial water bodies were manually appended. Figure 1C shows the study area for which postediting was carried out.

Additionally, in order to analyze the relationship between topographical parameters and glacier area, the watershed was delineated based on the SRTM DEM using the hydrology analysis tool in ArcGIS 9.3 and modified manually to obtain the drainage divides. Individual glaciers can be obtained by intersecting glacier and drainage polygons and then calculating topographic parameters (mean elevation, mean slope, and mean aspect) for each glacier entity by zonal statistics.

Error analysis

There are three main types of errors in mapping glacier outlines: technical errors, methodological or interpretation errors, and algorithm errors (Paul and Andreassen 2009). Assessing these errors is difficult, primarily because of the lack of sufficient ground-control points measured by differential global positioning system (DGPS) (Racoviteanu et al 2009). Methods of evaluating error include the error matrix (Gjermundsen et al 2011).

In this study, it was difficult to select the threshold for NDSI, because a glacier in shadow has a reflectance similar to that of bright rock. If the threshold is too low, shaded glaciers can be delineated automatically, but many rocks are included; 0.5 for NDSI is a balance trick. Seasonal snow is another factor producing error. If snow is not connected to a glacier, much of it can be removed by filter for areas smaller than 0.01 km^2. However, large snow patches classified as part of glaciers cannot be

http://dx.doi.org/10.1659/MRD-JOURNAL-D-12-00074.1

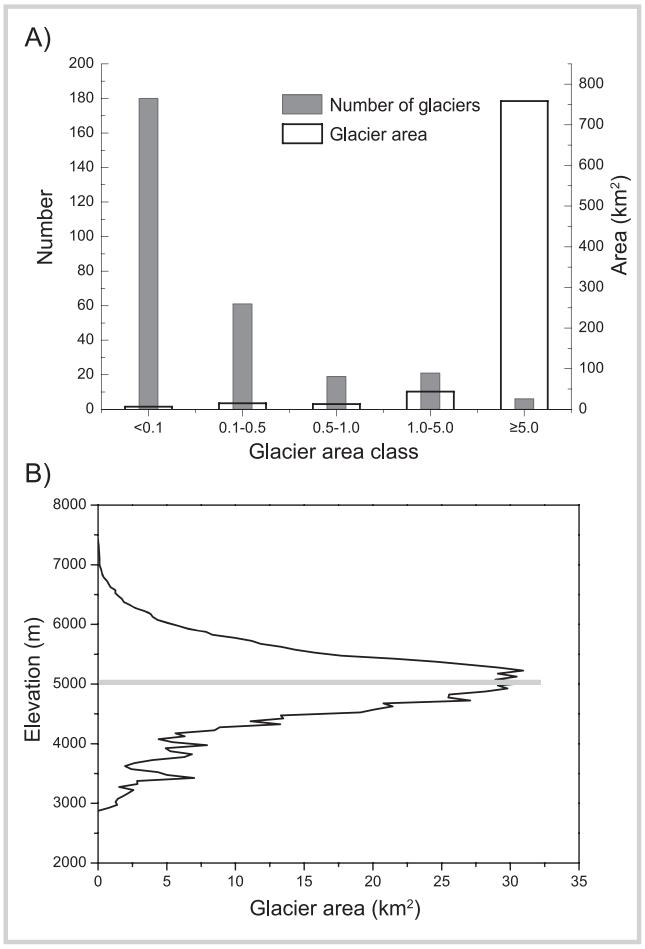

FIGURE 3 Glacier area, 1992. (A) Area and numbers per area class for 287 glaciers. (B) Area compared to elevation; the gray bar shows the equilibrium line altitude (ELA). To simplify the figure, the 50-m intervals were deleted from the y axis.

removed automatically, and deleting them manually would involve arbitrary choices. Although the remote-sensing images were acquired at the end of the ablation season, it is possible that it snowed some hours before the satellite passed over the area. In a positive mass balance year, seasonal snow can lead to greater error in delineating glacier areas (Gjermundsen et al 2011). A debris-covered glacier can also only be delineated with great uncertainty; it is very difficult to define its boundary, even if it is investigated on the spot. Because ALOS/AVNIR2 images have no SWIR band, errors were also caused by laborious manual delineation and editing.

Considering all these factors, three areas were selected on a classification map for Landsat TM/ETM+; each area included 400 pixels. There were 1, 2, and 4 pixels that could not be classified with certainty as glacier; thus, the glacier areas in 1992 and 2000 had an error of 0.5% at the confidence level of 95% based on the De Moivre–Laplace theorem in probability theory. Using the methods described earlier herein, we identified 5, 5, and 7 pixels in three areas on the ALOS classification map that could not clearly be classified as glaciers; thus, the glacier area in 2006 had a 1.1% error at the confidence level of 95%. The results were confirmed by hypothesis testing at the 0.05 significance level.

Results and discussion

There are 287 glaciers in the Fedchenko basin. Figure 3A shows the distribution of glacier areas and number of glaciers in 1992 per area class in the basin. Glaciers smaller than 1 km^2 make up 90.6% of the total number but only 4.1% of the total area. In contrast, glaciers larger than 5 km^2 make up 2.1% of the total number and 90.7%

TABLE 3 Glacier area change in the Fedchenko basin from 1992 to 2006.

Year	1992	2000	2006
Total glacier area (km^2)	835.9 ± 4	830.0 ± 4	864.8 ± 10
Period	**1992–2000**	**2000–2006**	**1992–2006**
Change in area (km^2)	−5.9 ± 4	+34.8 ± 10	+28.9 ± 10
Rate of change (%)	−0.71 ± 0.48	+4.19 ± 1.2	+3.46 ± 1.2
Rate of change (% per year)	−0.09 ± 0.06	+0.7 ± 0.2	+0.25 ± 0.08
Area of specific glaciers (km^2)	**1992**	**2006**	**Rate of change (%)**
Fedchenko	697.70	708.86	1.60
Kosinenko	23.20	27.26	17.50
Kalinina	17.70	18.20	2.80
Ulugbeka	9.10	9.76	7.30
Seismologov	5.60	6.20	10.80

http://dx.doi.org/10.1659/MRD-JOURNAL-D-12-00074.1

FIGURE 4 Slope, elevation, aspect, and area values, 1992. (A) Mean slope in relation to size. (B) Mean elevation in relation to mean aspect; the red quadratic polynomial curve fitting indicates glacier elevation trend against aspect.

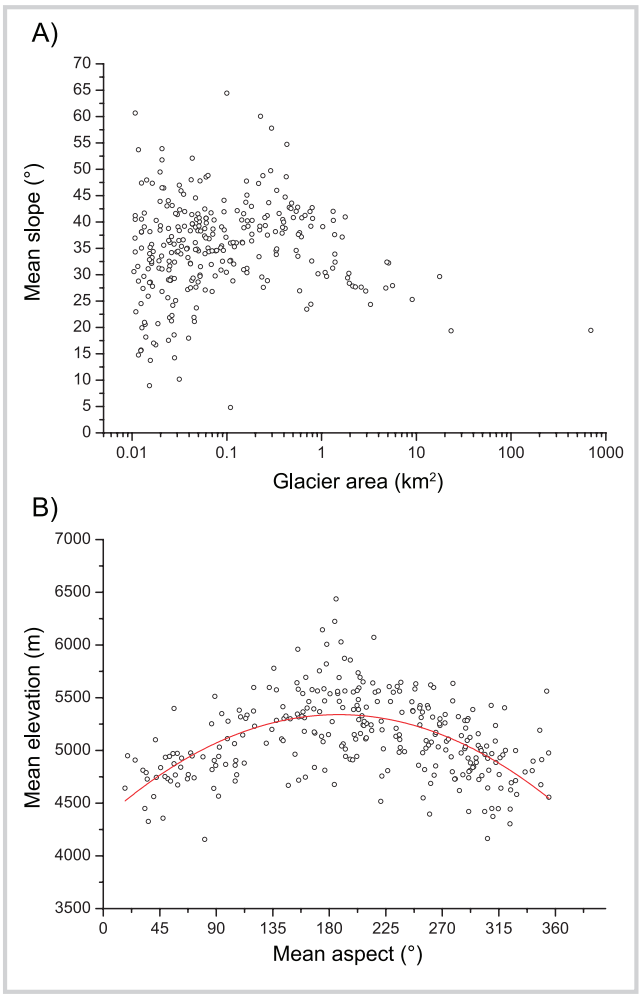

FIGURE 5 Change in area compared to initial area for 127 glaciers, 1992–2006.

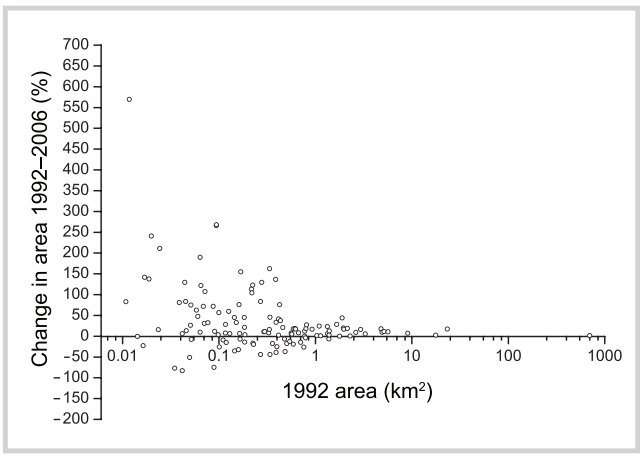

of the total area. The area class is bigger, the number of glaciers is smaller, and the total area is larger. The largest five are the Fedchenko, Kosinenko, Kalinina, Ulugbeka, and Seismologov glaciers, with areas of 697.7 km^2, 23.2 km^2, 17.7 km^2, 9.1 km^2, and 5.6 km^2, respectively (Table 3). Figure 3B presents the area–elevation distribution in 1992 by 50 m elevation intervals. The long-term ELA is approximately equal to the elevation for total maximum glacier area (Braithwaite and Raper 2009). The hypsography of glacierized areas indicates that the largest area lies in the range from 5000 m to 5050 m; thus, the ELA in the glacier system is close to 5000 m.

The relationship between glacier area and mean slope (Figure 4A) suggests that glaciers with a larger area have a smaller mean slope. Glaciers with a smaller area possess both more and less pronounced mean slopes, indicating a larger variability of slope for small glaciers than for large ones. The variation of glacier mean elevation against mean aspect (Figure 4B) suggests that glacier mean elevation is dependent on the aspect. Generally, the elevation of south-facing glaciers is higher; this may be mainly caused by solar radiation.

Figure 5 compares changes in glacier area between 1992 and 2006 to initial area for 127 selected glaciers, suggesting that both the relative change in area and the variation in that change increase in inverse proportion to the original glacier area. There was a larger scatter for glacier areas smaller than 1 km^2. Many small glaciers grew by more than 20%; some even increased by more than 100%, possibly by merging with other small glaciers. The finding of more than 500% change over 14 years is very unrealistic and was more likely caused by the presence of seasonal snow. The change in area of most glaciers ranged from −51% to +48%. Glaciers smaller than 1 km^2 either lost (up to 1.80 km^2) or gained (up to 7.08 km^2) area (the net gain was 5.28 km^2), whereas glaciers larger than 1 km^2 almost all gained area. The Fedchenko, Kosinenko, Kalinina, Ulugbeka, and Seismologov glaciers gained 11.16 km^2, 4.06 km^2, 0.50 km^2, 0.66 km^2, and 0.6 km^2, respectively (Table 3). The area gain for the Kosinenko glacier is prominent because of its surging. Absolute area gain was higher for larger glaciers. This implies that relative area change depends on glacier size (Bolch, Yao, et al 2010).

The total glacier areas in 1992, 2000, and 2006 are presented in Table 3. The uncertainty is ±0.5% (or ±4 km^2) for 1992 and 2000 and ±1.1% (or ±10 km^2) for 2006. The area diminished by 0.71% from 1992 to 2000 but enlarged by 4.19% from 2000 to 2006, for a gain of 3.46% from 1992 to 2006 (Figure 6). Two areas in particular changed remarkably:

1. The Vasilevskogo glacier advanced to connect with its trunk glacier in 2006, forming the shape of a paw, with a surging area of 0.2 km^2. The upper part of the main trunk of the Bivouac glacier surged after 1992 (Kotlyakov et al 2008) and is now in a quiescent phase; the surging belt can be discerned by comparing images

http://dx.doi.org/10.1659/MRD-JOURNAL-D-12-00074.1

FIGURE 6 Change in area of the Fedchenko glacier system, 1992–2006. (1) Vasilevskogo surging glacier; (2) Kosinenko surging glacier.

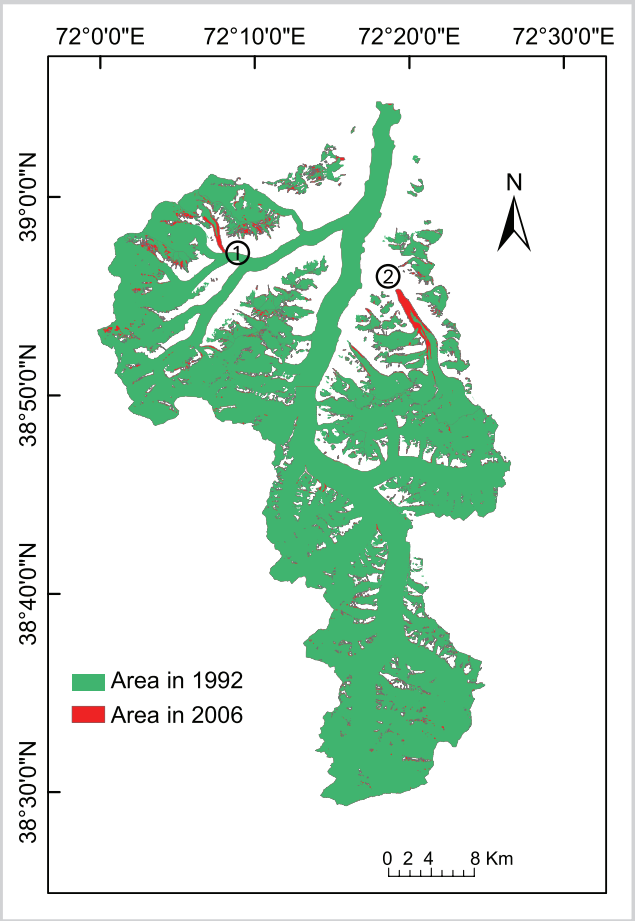

FIGURE 7 Summer temperature and winter precipitation since 1970 in the Fedchenko glacier system. (Reanalysis data from NCEP/NCAR)

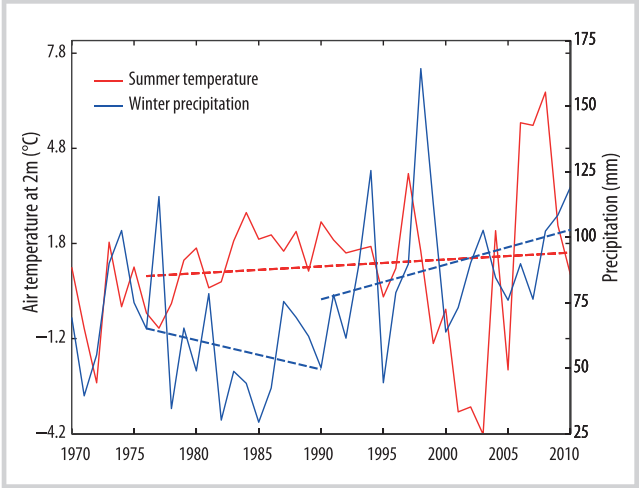

from 1992 and 2000. This part also surged from 1975 to 1978 (Kotlyakov et al 2008).

2. The Kosinenko glacier surged to 2280 m and enlarged by 3.5 km^2 between 2000 and 2006; however, the surging time cannot be determined precisely from the two remote-sensing images.

In addition to the surging area of 3.7 km^2, glacier area increased by another 25.2 km^2 from 1992 to 2006. Taking into account the delineating errors, glaciers in the Fedchenko basin are in a stable state. This result is in agreement with the mass balance of 0.00 ± 0.08 m y^{-1} water equivalent for the Fedchenko glacier between 2000 and 2011, and with the mass balance of surge-type and non-surge-type glaciers in Pamir, with +0.20 ± 0.24 m y^{-1} water equivalent and +0.13 ± 0.037 m y^{-1} water equivalent, respectively, during the same time (Gardelle et al 2013).

The glacier fluctuations could be linked to climate change. The Fedchenko glacier meteorological station has been closed since 1994; thus, reanalysis data (eg for temperature and precipitation) from the US National Centers for Environmental Prediction and National Center for Atmospheric Research (NCEP/NCAR) were used to investigate climate change in the region. The climate changes recorded by NCEP/NCAR (Figure 7) before 1994 follow the same trend as observed by the Fedchenko glacier meteorological station (Khromova et al 2006) for that period, which gives us confidence in using NCEP/NCAR data to interpret glacier changes.

Summer temperatures have not displayed a clear warming trend since 1970 (Figure 7); however, precipitation in winter decreased markedly from 1975 to 1990 and increased from 1990 to 2010. Glacier area responds more slowly to annual meteorological conditions than mass balance does (Cuffey and Paterson 2010). The adaptation of temperate glaciers to a mass change takes several years to several decades (Lopez et al 2010). With increasing precipitation in winter and almost stable temperatures in summer since 1990, the glaciers in the Fedchenko basin shrank slightly from 1992 to 2000, and then expanded after 2000. Therefore, increased winter precipitation is probably the major reason for slight glacier expansion in the last decade, which is consistent with the report of Yao et al (2012).

Conclusion

We used the NDSI method for TM/ETM+ images and the B4R2/4 method for an ALOS/AVNIR2 image to extract the area of the Fedchenko glacier system, and we divided this into individual glaciers through the drainage divide method. Glacier area increased and glacier numbers decreased with increasing glacier area. The mean slope decreased when the area increased, and smaller glaciers showed a larger variability in slope. The altitude for maximal area ranges from 5000 to 5050 m asl; thus, the ELA in the glacier system is around 5000 m. Glacier elevation is larger when facing south.

http://dx.doi.org/10.1659/MRD-JOURNAL-D-12-00074.1

Results also show that larger glaciers have less relative change in area, and smaller glaciers have a greater range of variability. Total glacier area in the basin shrank 5.9 km^2 (0.71%) from 1992 to 2000 and expanded 34.8 km^2 (4.19%) from 2000 to 2006, for an increase in total area of 28.9 km^2 (3.46%) from 1992 to 2006—a slight expansion after excluding errors and glacier surging. With a continuous increase in winter precipitation since 1990, glaciers retreated slowly at first, and then advanced beginning in 2000, when they adjusted to positive mass balance. Increasing precipitation probably represents the controlling factor for glacier variations in this region.

ACKNOWLEDGMENTS

We thank two anonymous reviewers and the editors for their valuable comments, which greatly improved the manuscript. This study was supported by the Global Change Research Program of China (2010CB951401), the National Natural Science Foundation of China (41121001, 41190081, 41225002), and State Key Laboratory of Cryospheric Sciences (SKLCS-ZZ-2013-01-01).

REFERENCES

Aizen VB, Mayewski PA, Aizen EM, Joswiak DR, Surazakov AB, Kaspari S, Grigholm B, Krachler M, Handley M, Finaev A. 2009. Stable-isotope and trace element time series from Fedchenko glacier (Pamirs) snow/firn cores. *Journal of Glaciology* 55(190):275–291.

Andreassen LM, Paul F, Kääb A, Hausberg JE. 2008. Landsat-derived glacier inventory for Jotunheimen, Norway, and deduced glacier changes since the 1930s. *The Cryosphere* 2:131–145.

Barnett TP, Adam JC, Lettenmaier DP. 2005. Potential impacts of a warming climate on water availability in snow-dominated regions. *Nature* 438(7066): 303–309.

Bayr KJ, Hall DK, Kovalick WM. 1994. Observations on glaciers in the eastern Austrian Alps using satellite data. *International Journal of Remote Sensing* 15(9):1733–1742.

Bolch T, Menounos B, Wheate R. 2010. Landsat-based inventory of glaciers in western Canada, 1985–2005. *Remote Sensing of Environment* 114:127–137.

Bolch T, Yao T, Kang S, Buchroithner MF, Scherer D, Maussion F, Huintjes E, Schneider C. 2010. A glacier inventory for the western Nyainqentanglha Range and the Nam Co Basin, Tibet, and glacier changes 1976–2009. *The Cryosphere* 4:419–433.

Braithwaite RJ. 1984. Can the mass balance of a glacier be estimated from its equilibrium-line altitude. *Journal of Glaciology* 30(106):364–368.

Braithwaite RJ, Raper SCB. 2009. Estimating equilibrium-line altitude (ELA) from glacier inventory data. *Annals of Glaciology* 53(50):127–132.

Chavez PS. 1988. An improved dark-object subtraction technique for atmospheric scattering correction of multispectral data. *Remote Sensing of Environment* 24:459–479.

Consultative Group for International Agriculture Research's Consortium for Spatial Information. 2013. SRTM 90 m Digital Elevation Data. srtm.csi.cgiar.org; accessed in August 2012.

Cuffey KM, Paterson WSB. 2010. *The physics of glaciers.* 4th edition 2010. New York: Elsevier Science.

Dozier J. 1989. Spectral signature of alpine snow cover from the Landsat Thematic Mapper. *Remote Sensing of Environment* 28:9–22.

Gardelle J, Berthier E, Arnaud Y. 2012. Slight mass gain of Karakoram glaciers in the early twenty-first century. *Nature Geoscience* 5:322–325. http://dx.doi.org/10.1038/ngeo1450.

Gardelle J, Berthier E, Arnaud Y, Kääb A. 2013. Region-wide glacier mass balances over the Pamir-Karakoram-Himalaya during 1999–2011. *The Cryosphere Discussion* 7:975–1028.

Gjermundsen EF, Mathieu R, Kääb A, Chinn T, Fitzharris B, Hagen JO. 2011. Assessment of multispectral glacier mapping methods and derivation of glacier area changes, 1978–2002, in the central Southern Alps, New Zealand, from ASTER satellite data, field survey and existing inventory data. *Journal of Glaciology* 57(204):667–683.

Global Land Cover Facility. 2013. Global Land Cover Facility. www.glcf.umiacs.umd.edu/data/; accessed in August 2012.

Gupta RP, Haritashya UK, Singh P. 2005. Mapping dry/wet snow cover in the Indian Himalayas using IRS multispectral imagery. *Remote Sensing of Environment* 97:458–469.

Haeberli W. 1995. Glacier fluctuations and climate change detection. *Geografia Fisica e Dinamica Quaternaria* 18:191–199.

Hall DK, Riggs GA, Salomonson VV. 1995. Development of methods for mapping global snow cover using moderate resolution imaging spectroradiometer data. *Remote Sensing of Environment* 54:127–140.

Haritashya UK, Bishop MP, Shroder JF, Bush ABG, Bulley HNN. 2009. Space-based assessment of glacier fluctuations in the Wakhan Pamir, Afghanistan. *Climatic Change* 94:5–18.

Jacobs JD, Simms EL, Simms A. 1997. Recession of the southern part of Barnes ice cap, Baffin Island, Canada, between 1961 and 1993, determined from digital mapping of Landsat TM. *Journal of Glaciology* 43(143):98–102.

Japan Aerospace and Exploration Agency. 2006. Earth Observation Research Center: Seen from Space: Gigantic Glacier in Pamir Mountains: Fedchenko Glacier. www.eorc.jaxa.jp/en/imgdata/topics/2006/tp060703.html; accessed in August 2012.

Kääb A. 2008. Glacier volume changes using ASTER satellite stereo and ICESat GLAS laser altimetry. A test study on Edgeøya, eastern Svalbard. *IEEE Transactions on Geoscience and Remote Sensing* 46(10):2823–2830.

Kang S, Xu Y, You Q, Flügel WA, Pepin N, Yao T. 2010. Review of climate and cryospheric change in the Tibetan Plateau. *Environmental Research Letter* 5: 015101. http://dx.doi.org/10.1088/1748-9326/5/1/015101.

Kargel JS, Abrams MJ, Bishop MP, Bush A, Hamilton G, Jiskoot H, Kääb A, Kieffer HH, Lee EM, Paul F, Rau F, Raup B, Shroder JF, Soltesz D, Stainforth D et al. 2005. Multispectral imaging contributions to global land ice measurements from space. *Remote Sensing of Environment* 99:187–219.

Khromova TE, Osipova GB, Tsvetkov DG, Dyurgerov MB, Barry RG. 2006. Changes in glacier extent in the eastern Pamir, Central Asia, determined from historical data and ASTER imagery. *Remote Sensing of Environment* 102:24–32.

Kotlyakov VM, Osipova GB, Tsvetkov DG. 2008. Monitoring surging glaciers of the Pamirs, central Asia, from space. *Annals of Glaciology* 48:125–134.

Kulkarni AV. 1992. Mass balance of Himalayan glaciers using AAR and ELA methods. *Journal of Glaciology* 38(128):101–104.

Kutuzov S, Shahgedanova M. 2009. Glacier retreat and climatic variability in the eastern Terskey-Alatoo, inner Tien Shan between the middle of the 19th century and beginning of the 21st century. *Global and Planetary Change* 69:59–70.

Le Bris R, Paul F, Frey H, Bolch T. 2011. A new satellite-derived glacier inventory for western Alaska. *Annals of Glaciology* 52(59):135–143.

Lopez P, Chevallier P, Favier V, Pouyaud B, Ordenes F, Oerlemans J. 2010. A regional view of fluctuations in glacier length in southern South America. *Global and Planetary Change* 71:85–108.

Micklin P. 2006. The Aral Sea disaster. *Annual Review of Earth and Planetary Sciences* 35(1):47–72.

Oerlemans J. 1994. Quantifying global warming from the retreat of glaciers. *Science* 264(5156):243–245.

Oerlemans J. 2001. *Glaciers and Climate Change*. Rotterdam, Netherlands: Balkema Publishers.

Paul F. 2000. *Evaluation of Different Methods for Glacier Mapping Using Landsat TM.* EARSeL [European Association of Remote Sensing Laboratories]-LISSIG-Workshop of Land Ice and Snow Proceedings. EARSeL eProceedings Vol. 1, No. 1. Dresden, Germany: European Association of Remote Sensing Laboratories, pp 239–245.

Paul, F. 2002. Changes in glacier area in Tyrol, Austria, between 1969 and 1992 derived from Landsat 5 thematic mapper and Austrian Glacier Inventory data. *International Journal of Remote Sensing* 23(4):787–799.

Paul F, Andreassen LM. 2009. A new glacier inventory for the Svartisen region, Norway, from Landsat ETM+ data: Challenges and change assessment. *Journal of Glaciology* 55(192):607–618.

Paul F, Huggel C, Kääb A. 2004. Combining satellite multispectral image data and a digital elevation model for mapping debris-covered glaciers. *Remote Sensing of Environment* 89:510–518.

Paul F, Kääb A, Haeberli W. 2007. Recent glacier changes in the Alps observed by satellite: Consequences for future monitoring strategies. *Global and Planetary Change* 56:111–122.
Paul F, Kääb A, Maisch M, Kellenberger T, Haeberli W. 2002. The new remote sensing derived Swiss glacier inventory: I. Methods. *Annals of Glaciology* 34: 355–361.
Racoviteanu AE, Arnaud Y, Williams MW, Ordoñez J. 2008. Decadal changes in glacier parameters in the Cordillera Blanca, Peru, derived from remote sensing. *Journal of Glaciology* 54(186):499–510.
Racoviteanu AE, Paul F, Raup B, Khalsa SJS, Armstrong R. 2009. Challenges and recommendations in mapping of glacier parameters from space: Results of the 2008 Global Land Ice Measurements from Space (GLIMS) workshop, Boulder, Colorado, USA. *Annals of Glaciology* 50(53):53–69.
Racoviteanu AE, Williams MW, Barry RG. 2008. Optical remote sensing of glacier characteristics: A review with focus on the Himalaya. *Sensors* 8:3355–3383.
Raup B, Racoviteanu A, Khalsa SJS, Helm C, Armstrong R, Arnaud Y. 2007. The GLIMS geospatial glacier database: A new tool for studying glacier change. *Global and Planetary Change* 56(1–2):101–110.
Sandmeier S, Itten KI. 1997. A physically-based model to correct atmospheric and illumination effects in optical satellite data of rugged terrain. *IEEE Transactions on Geoscience and Remote Sensing* 35(3):708–717.
Silverio W, Jaquet JM. 2005. Glacial cover mapping (1987–1996) of the Cordillera Blanca (Peru) using satellite imagery. *Remote Sensing of Environment* 95:342–350.
Song C, Woodcock CE, Seto KC, Lenney MP, Macomber SA. 2001. Classification and change detection using Landsat TM data: When and how to correct atmospheric effects? *Remote Sensing of Environment* 75:230–244.
Svoboda F, Paul F. 2009. A new glacier inventory on southern Baffin Island, Canada, from ASTER data: I. Applied method, challenges and solutions. *Annals of Glaciology* 50(53):11–21.
Warren SG. 1982. Optical properties of snow. *Reviews of Geophysics and Space Physics* 20(1):67–89.
Willis MJ, Melkonian AK, Pritchard ME, Ramage JM. 2012. Ice loss rates at the northern Patagonian icefield derived using a decade of satellite remote sensing. *Remote Sensing of Environment* 117:184–198.
Winther JG. 1992. Landsat Thematic Mapper (TM) derived reflectance from a mountainous watershed during the snow melt season. *Nordic Hydrology* 23: 273–290.
Yao T, Thompson L, Yang W, Yu W, Gao Y, Guo X, Yang X, Duan K, Zhao H, Xu B, Pu J, Lu A, Xiang Y, Kattel DB, Joswiak D. 2012. Different glacier status with atmospheric circulations in Tibetan Plateau and surroundings. *Nature Climate Change* 2:663–667. http://dx.doi.org/10.1038/nclimate1580.